IOPscience iopscience.iop.org

Home Search Collections Journals About Contact us My IOPscience

Fractal structure in optical spectra of Fibonacci superlattices

This article has been downloaded from IOPscience. Please scroll down to see the full text article.

1994 J. Phys.: Condens. Matter 6 4107

(http://iopscience.iop.org/0953-8984/6/22/010)

View the table of contents for this issue, or go to the journal homepage for more

Download details:
IP Address: 171.66.16.147
The article was downloaded on 12/05/2010 at 18:31

Please note that terms and conditions apply.

J. Phys.: Condens. Matter 6 (1994) 4107–4118. Printed in the UK

Fractal structure in optical spectra of Fibonacci superlattices

D Munzar†, L Bočáek†, J Humlíček† and K Ploog‡

† Department of Solid State Physics, Faculty of Science, Masaryk University Kotlářská 2, 61137 Brno, Czech Republic

‡ Paul-Drude-Institut für Kestkörperelektronik, Hausvogteiplatz 5-7, 1086 Berlin, Germany

Received 21 December 1993

Abstract. We present the results of theoretical and experimental studies of GaAs/GaAlAs Fibonacci superlattices. The normal-incidence reflectance was measured for a Fibonacci superlattice in the temperature range from 20 to 300 K. We develop a simple model to predict the reflectance theoretically. The energy levels are calculated with the help of the envelope-function approximation and the Kohmoto–Kadanoff–Tang renormalization-group method. The model predictions are in good agreement with the experiment. The electronic structure of Fibonacci superlattices exhibits multifractal properties, which manifest themselves also in the experimental reflectance spectra.

1. Introduction

There is much current interest in quasicrystals, i.e., solids intermediate between completely periodic crystals and random or disordered amorphous solids [1]. The linear lattices constructed recursively as follows: $S_{j+1} = \{S_j S_{j-1}\}$ for $j > 0$, with $S_0 = \{B\}$ and $S_1 = \{A\}$, are called Fibonacci lattices (FLs). They represent a simple type of one-dimensional quasicrystal. For this reason they have been subject of intensive theoretical studies. The electronic structure of FLs is usually studied in the frame of a tight-binding model with arbitrary on-site energies corresponding to the sites A and B and arbitrary hopping-matrix elements between the sites A–A and A–B (see, e.g., [2] and references therein). The energy spectrum of an infinite FL is singularly continuous with zero Lebesque measure: the set of energy gaps is a dense set and there is no isolated energy level. The wave functions are critical in the sense that they are neither extended nor localized [2].

Molecular-beam epitaxy opens a possibility to prepare FLs artificially. These so called Fibonacci superlattices (FSLs) consist of two layers A and B alternating according to the Fibonacci rule. The layers A and B are usually composed of several monolayers (mL) of GaAs and $Ga_{1-x}Al_xAs$. FSLs were grown for the first time by Merlin and co-workers in 1985 [3]; this was followed by a fairly high activity in this field [4].

The optical properties of GaAs/GaAlAs FSLs in the near infrared were studied by means of ellipsometry [5, 6] and by means of photoluminescence excitation (PLE) spectroscopy [7, 8]. The results were interpreted qualitatively in terms of the (single band) envelope-function approximation (EFA) [9] which is known to be quite successful in the case of periodic GaAs/GaAlAs superlattices. The hybridization effects in FSLs studied recently by Hirose *et al* [10] with the help of the semi-empirical sp^3s^* tight-binding method [11] do not influence significantly the electronic structure in the region close to the fundamental gap.

Garriga and co-workers [5, 6] calculated the interband continuum in the imaginary part of the dielectric function ϵ_2 and suggested a correspondence between the steps in the

theoretical lineshapes and the peaks observed in the ellipsometric spectra. Laruelle and Etienne [7] compared the positions of the structures of the PLE spectra with the calculated values of the transition energies and Yamaguchi *et al* [8] compared their PLE spectra with the calculated density of states corresponding to the conduction-band electrons. The partial agreement between the experimental results and the theoretical predictions in the quoted works concerns only the energies of the most pronounced spectral structures.

In this paper we report the analysis of the normal-incidence reflectance spectra of a GaAs/GaAlAs FSL in the temperature range from 20 to 300 K. The spectra are interpreted by comparing with the calculated reflectance. We aim at comparing not only the positions but also the shapes of the spectral structures. As far as we know it is the first time that the reflectance of an FSL in the region containing the onset of the interband absorption has been calculated. The multifractal structure of the electron energy spectrum is also drawn in the hierarchical form of the reflectance spectrum.

The paper is organized as follows. Section 2 contains a brief description of the sample and the experimental set-up. The method of calculation of the energy levels and the wave functions of electrons and holes in FSLs is presented in subsection 3.1. We have used the EFA and the Kohmoto–Kadanoff–Tang renormalization-group method [12]. The calculation of the dielectric function and the reflectance is described in subsection 3.2. A detailed comparison of the measured and calculated lineshapes is given in section 4.

2. Experiment

The FSL sample was grown by molecular-beam epitaxy on a (100) semi-insulating GaAs substrate. The nominal composition of the building blocks A and B was 6 mL of GaAs and 4 mL of $Ga_{0.65}Al_{0.35}As$ alloy, respectively.

The growth was stopped after finishing the 12th step of the recursive rule. The target thickness of the FSL film is 347 nm; the actual value measured ellipsometrically is (326 $\pm$ 13) nm. The measured refractive index at 633 nm, 3.787 $\pm$ 0.011, is somewhat higher than the value of 3.773 calculated within the effective-medium approximation [13] for the FSL with the nominal composition of the building blocks. This indicates that the portion of GaAs in the sample is higher (the refractive index of GaAs is higher than that of the alloy). We conclude that the deficiency observed in the total number of monolayers is due to the fact that the mean thickness of the barrier $B \simeq 3$ mL.

Reflectance spectra at near-normal incidence were measured, point by point, with photon energies between 1.4 eV and 1.8 eV in the temperature range from 20 to 300 K. A stable 150 W tungsten lamp was used to produce monochromatic light. The ratio of signals after reflection on the sample and a single-crystal silicon slice was multiplied by the known reflectance of silicon [14] to obtain the reflectivity of the sample on an absolute scale. We estimate the absolute accuracy and the mean noise level to be about 0.01 to 0.0003, respectively.

3. Theory

3.1. Electronic structure

In this section we present the method of calculation of the $k_\perp = 0$ energy levels and wave functions of electrons and heavy and light holes in FSLs. Our description concerns the FSLs with A = $(GaAs)_m$ and B = $(Ga_{1-x}Al_xAs)_n$ but the approach can be easily modified for

FSLs with another choice of building blocks. The most important results will be shown for the FSL with A = $(GaAs)_6$ and B = $(Ga_{0.65}Al_{0.35}As)_3$. The values of the parameters entering the calculation used in this case are given in table 1.

Within the EFA [9] the wave function of an electron in an FSL has the following form:

$$\psi(\boldsymbol{r}) = f_{l,i}(\boldsymbol{r})u_{l0}(\boldsymbol{r})$$

where $f_{l,i}(\boldsymbol{r})$ is the envelope function varying slowly over the unit cells and $u_{l0}(\boldsymbol{r})$ is the Bloch function corresponding to the Γ point in the Brillouin zone. Index l denotes the band from which the wave function originates; i represents the remaining quantum numbers.

For the $k_\perp = 0$ conduction band states, we have $\psi(\boldsymbol{r}) = f(z)u(\boldsymbol{r})$, where z is the coordinate perpendicular to the layers of the FSL and $u(\boldsymbol{r})$ is the Bloch function at Γ. The function $f(z)$ and the corresponding energy eigenvalue E obey the stationary Schrödinger equation:

$$\left\{-\frac{\hbar^2}{2m_0}\frac{\mathrm{d}}{\mathrm{d}z}\frac{1}{m(z)}\frac{\mathrm{d}}{\mathrm{d}z} + V(z)\right\} f(z) = Ef(z). \tag{1}$$

Here m_0 is the free-electron mass and $m(z)$ is the electron effective mass in units of m_0,

$$m(z) = \begin{cases} m_{\mathrm{A}} & \text{for } z \in A \\ m_{\mathrm{B}} & \text{for } z \in B \end{cases}.$$

$V(z)$ is the step potential,

$$V(z) = \begin{cases} 0 & \text{for } z \in A \\ V_{\mathrm{c}} & \text{for } z \in B \end{cases}.$$

V_{c} is the conduction band offset between $Ga_{1-x}Al_xAs$ and GaAs. The model potential at the beginning of the FSL (sequence ABAABABAABAAB) is shown in the upper part of figure 1.

The boundary conditions for equation (1) at the A–B and B–A interfaces are such that

$$f(z) \text{ and } \frac{1}{m(z)}\frac{\mathrm{d}f(z)}{\mathrm{d}z}$$

are both continuous.

We have solved equation (1) using the common transfer-matrix technique. The form of the transfer matrices will be briefly described.

Let us denote the z-coordinate of the nth interface by z_n. In the layer A situated between z_n and z_{n+1}, the envelope function can be written in two different ways:

$$f(z) = C_l \cos[k(z - z_n)] + S_l \sin[k(z - z_n)]$$

and

$$f(z) = C_r \cos[k(z - z_{n+1})] + S_r \sin[k(z - z_{n+1})]$$

where $k = \sqrt{2m_0 m_{\mathrm{A}} E/\hbar^2}$. C_r and S_r are connected with C_l and S_l through the transfer matrix:

$$\begin{pmatrix} C_r \\ S_r \end{pmatrix} = \begin{pmatrix} \cos(x) & \sin(x) \\ -\sin(x) & \cos(x) \end{pmatrix} \begin{pmatrix} C_l \\ S_l \end{pmatrix} \tag{2}$$

Table 1. The values of the parameters entering the calculation of the reflectance used for the FSL of order $n = 12$ with A = $(GaAs)_6$ and B = $(Ga_{0.65}Al_{0.35}As)_3$.

E_g	V_c	V_v	m_{elA}	m_{elB}	m_{hhA}	m_{hhB}	m_{lhA}	m_{lhB}	P^2/m_0	d
1.519 eV [24]	0.379 eV[a]	0.187 eV[a]	$0.067m_0$ [24]	$0.096m_0$[b]	$0.403m_0$ [16]	$0.405m_0$[b]	$0.087m_0$ [16]	$0.109m_0$[b]	11.35 eV [16]	326 nm[c]

$\mu_{el,hh}$	$\mu_{el,lh}$	$E_{exc,hh}$	$E_{exc,lh}$	B	γ	σ_0	C	F	E_0	Γ
$0.041m_0$	$0.051m_0$	10 meV	10 meV	1.51	1.4 meV	2 meV	12 meV^{-1}	170 eV^2	4.1 eV	0.20 eV

[a] The values are calculated from the band gaps of GaAs and $Ga_{0.65}Al_{0.35}As$ (2.085 eV) using the band-gap discontinuity ratio 67/33 [16]. The band gap of $Ga_{0.65}Al_{0.35}As$ was taken as the weighted average of the band gaps of GaAs and AlAs from [24].

[b] Weighted averages of the effective masses in GaAs and the effective masses in AlAs from [24].

[c] Our measured ellipsometric value.

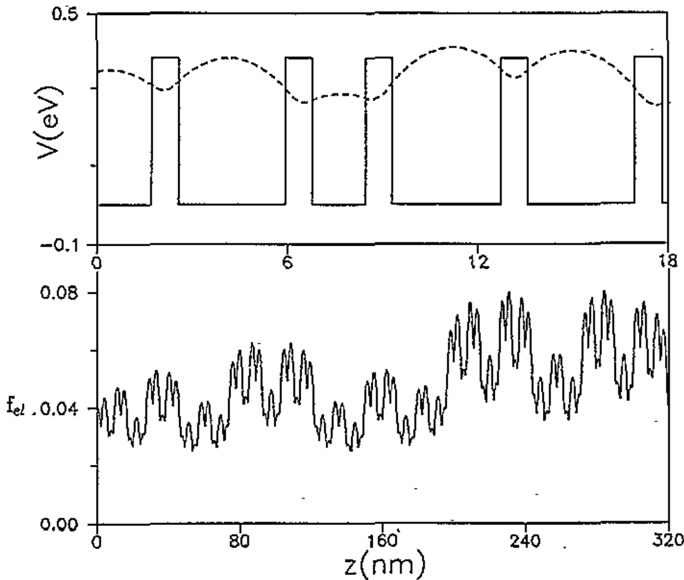

Figure 1. Upper part: model potential for electrons at the beginning of an FSL built from A = $(GaAs)_6$ and B = $(Ga_{0.65}Al_{0.35}As)_3$; z is the coordinate along the growth axis. Lower part: envelope wave function describing the ground state of electrons in the FSL S_{12}. A detail multiplied by a factor of eight is shown as the dashed line in the upper part.

where $x = ak$; a is the thickness of the layer A. Let us denote the matrix of equation (2) by $\mathbf{T}_A$.

Let z_n be the coordinate of an interface between layers A and B. For the layer A situated between z_{n-1} and z_n, we can write

$$f(z) = C_l \cos[k(z - z_n)] + S_l \sin[k(z - z_n)].$$

For the next layer A situated between z_{n+1} and z_{n+2}, we can write

$$f(z) = C_r \cos[k(z - z_{n+1})] + S_r \sin[k(z - z_{n+1})].$$

The boundary conditions yield

$$\begin{pmatrix} C_r \\ S_r \end{pmatrix} = \begin{pmatrix} \cosh(y) & xbm_B \sinh(y)/(yam_A) \\ yam_A \sinh(y)/(xbm_B) & \cosh(y) \end{pmatrix} \begin{pmatrix} C_l \\ S_l \end{pmatrix} \quad (3)$$

where $y = \sqrt{2m_0 m_B(V_c - E)/\hbar^2}$; b is the thickness of the layer B. Let us denote the matrix of equation (3) by $\mathbf{T}_B$.

The coefficients C_r and S_r representing the wave function at the end of the sequence S_n (FSL of the order n) can be calculated from the coefficients C_l and S_l representing it at the beginning of the FSL:

$$\begin{pmatrix} C_r \\ S_r \end{pmatrix} = \mathbf{T}_A \mathbf{T}_B \ldots \mathbf{T}_A \mathbf{T}_B \mathbf{T}_A \begin{pmatrix} C_l \\ S_l \end{pmatrix} \equiv \mathbf{T}_n \begin{pmatrix} C_l \\ S_l \end{pmatrix} \quad (4)$$

where the arrangement of the transfer matrices in $\mathbf{T}_n$ is reversed with respect to that of the layers A and B in the FSL.

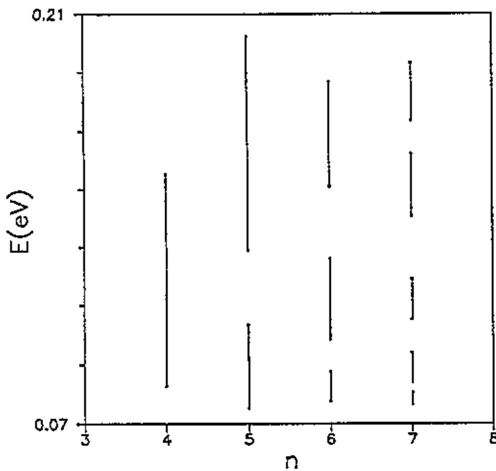

Figure 2. Energy bands of electrons in the periodic approximation $(S_n)_\infty$ to the infinite FSL as a function of the Fibonacci order n.

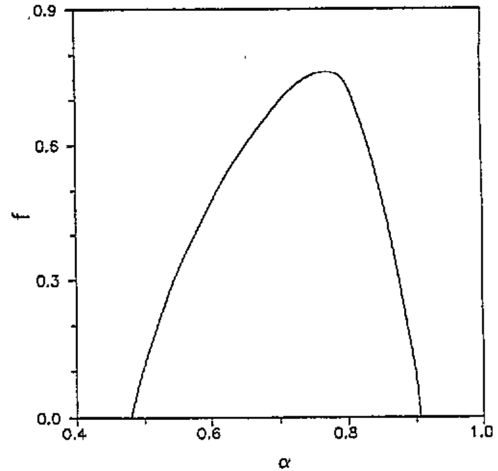

Figure 3. f–α curve for the electron energy spectrum of the infinite FSL.

The eigenvalue problem (1) has to be completed by proper boundary conditions. First, let us consider the hypothetical case of the infinite FSL (S_∞). S_∞ can be approximated by periodic sequences of the layers S_n, denoted by $(S_n)_\infty$. The higher the order n the better the approximation to the infinite FSL obtained. The wave function at the beginning of any layer S_n in $(S_n)_\infty$ can differ from the wave function at the end of it only by a phase factor:

$$\begin{pmatrix} C_r \\ S_r \end{pmatrix} = e^{i\phi} \begin{pmatrix} C_l \\ S_l \end{pmatrix}. \tag{5}$$

By inserting this condition in equation (4) we obtain

$$\mathrm{Tr}\left(\mathbf{T}_n\right) = 2\cos(\phi). \tag{6}$$

The last equation determines the energy spectrum (note that the elements of $\mathbf{T}_n$ depend on energy). For the allowed energies, $|\mathrm{Tr}(\mathbf{T}_n)| \leqslant 2$. Because of the quasiperiodicity we need not to multiply all the matrices involved in $\mathbf{T}_n$ when solving equation (6). Let us define $x_n = \mathrm{Tr}(\mathbf{T}_n)/2$. The x_n obey the recursive rule [12]:

$$x_{n+3} = 2x_{n+2}x_{n+1} - x_n \tag{7}$$

which allows us to calculate $\mathrm{Tr}\mathbf{T}_n)$ starting from x_0, x_1, and x_2.

The energy bands of electrons in the periodic approximations $(S_4)_\infty$, $(S_5)_\infty$, $(S_6)_\infty$, and $(S_7)_\infty$ to S_∞ are shown in figure 2. We have analysed the scaling properties of the energy spectrum of S_∞ in the same way as was done in [2]. Let E be in the energy spectrum. The spectrum is said to have a scaling at E with a scaling index α if the integrated density of states D behaves as

$$D(E+\Delta E) - D(E) \sim (\Delta E)^\alpha \qquad \text{as } \Delta E \to 0.$$

The fractal dimension f of the set of energies with a given α as a function of α [15] is shown in figure 3. The maximum of $f(\alpha)$ is the fractal dimension of the energy spectrum.

We have calculated also the energy levels in the case of the finite FSL S_{12} using the cyclic boundary conditions, $\phi = 0$ in equation (5). The eigenfunctions can be readily calculated using the transfer matrices of equation (2) and equation (3) throughout the stack of the layers. The wave function of the ground state of electrons in the FSL S_{12} is shown in the lower part of figure 1. Note the self-similarity of the wave.

The energy eigenvalues and the wave functions of heavy and light holes in the $k_\perp = 0$ case were calculated in the same manner. We replaced V_c in equation (1) by the negatively taken valence-band offset between $Ga_{1-x}Al_xAs$ and GaAs V_v and the electron effective masses by the corresponding hole effective masses.

3.2. *Optical properties*

The optical properties of the FSLs are treated using the formalism common in the cases of simple quantum wells and periodic superlattices summarized in [9]. The energy eigenvalues of electrons, heavy holes, and light holes and the corresponding envelope wave functions are denoted by $\{E_{\mathrm{el},i}\}$, $\{E_{\mathrm{hh},i}\}$, $\{E_{\mathrm{lh},i}\}$, and $\{f_{\mathrm{el},i}\}$, $\{f_{\mathrm{hh},i}\}$, $\{f_{\mathrm{lh},i}\}$, respectively; i is the index variable.

First we present the formulas for the imaginary part $\epsilon_2(E)$ of the dielectric function at the photon energy E. It can be decomposed into two parts: the contribution of the continuum $\epsilon_{2\mathrm{C}}(E)$ and the contribution of the discrete exciton states $\epsilon_{2\mathrm{exc}}(E)$

$$\epsilon_2(E) = \epsilon_{2\mathrm{C}}(E) + \epsilon_{2\mathrm{exc}}(E).$$

The former can be calculated analytically using the assumptions of EFA and assuming further that the selection rules

$$\left| \int f^*_{\mathrm{el},i}(z) f_{\mathrm{hh},j} \mathrm{d}r \right|^2 = \delta_{i,j} \qquad \left| \int f^*_{\mathrm{el},i}(z) f_{\mathrm{lh},j} \mathrm{d}r \right|^2 = \delta_{i,j} \tag{8}$$

are valid:

$$\epsilon_{2\mathrm{C}}(E) = \frac{Q}{E^2} \left\{ \mu_{\mathrm{el,hh}} \sum_i \Theta(E - E_g - E_{\mathrm{el},i} - E_{\mathrm{hh},i}) + \frac{1}{3} \mu_{\mathrm{el,hh}} \sum_i \Theta(E - E_g - E_{\mathrm{el},i} - E_{\mathrm{lh},i}) \right\} \tag{9}$$

where $Q = e^2 P^2 (2m_0^2 d)$. $P = -\mathrm{i}\langle S|p_x|X\rangle$ is the matrix element between the valence band p state at Γ and the conduction band s state at Γ for GaAs; d is the FSL thickness; $\mu_{\mathrm{el,hh}}$ and $\mu_{\mathrm{el,lh}}$ are reduced 'in plane' effective masses of the electron–heavy-hole and electron–light-hole pairs in GaAs, respectively; E_g is the energy gap of GaAs. $\Theta(x)$ is the step function. The values of $\mu_{\mathrm{el,hh}}$ and $\mu_{\mathrm{el,lh}}$ listed in table 1 were calculated using the formulas for the 'in plane' hole effective masses: $1/m_{\mathrm{hh},\perp} = \gamma_1 + \gamma_2 + P^2/(m_0 E_g)$, $1/m_{\mathrm{lh},\perp} = \gamma_1 - \gamma_2 + P^2/(3m_0 E_g)$, with the values of the Luttinger parameters γ_1 and γ_2 taken from [16]. In order to avoid the shape edges in the spectra, the step function in equation (9) was replaced by the error function

$$\frac{1}{\sqrt{2\pi}\gamma} \int_{-\infty}^{x} \exp\left(-t^2/(2\gamma^2)\right) \mathrm{d}t$$

resulting from the Gaussian broadening with a phenomenological width γ. The contribution of discrete exciton states can be calculated analytically on the assumptions given above only

in the two-dimensional (2D) model [17]. In that case

$$\epsilon_{2\text{exc}}(E) = \frac{8Q}{E^2}\left\{\mu_{\text{el,hh}} R_{\text{exc,hh}} \sum_i \delta\big(E - E_{\text{g}} - E_{\text{el},i} - E_{\text{hh},i} + R_{\text{exc,hh}}\big) + \frac{1}{3}\mu_{\text{el,lh}} R_{\text{exc,lh}} \sum_i \delta\big(E - E_{\text{g}} - E_{\text{el},i} - E_{\text{lh},i} + R_{\text{exc,lh}}\big)\right\}. \tag{10}$$

Here $R_{\text{exc,hh}} = \mu_{\text{el,lh}} e^4/(8\pi^2\epsilon^2\hbar^2)$ and $R_{\text{exc,lh}} = \mu_{\text{el,lh}} e^4/(8\pi^2\epsilon^2\hbar^2)$ are heavy- and light-hole 2D exciton rydbergs, respectively, and only the lowest discrete exciton states are taken into account. In the case of the FSL, the exciton states are far from 2D because of considerable coupling between the states centred in different wells. For this reason, and in order to describe phenomenologically the broadening of the excitonic lines, we have modified equation (10) in the following way:

$$\epsilon_{2\text{exc}}(E) = \frac{8BQ}{E^2\sqrt{2\pi}\sigma}\left\{\mu_{\text{el,hh}} E_{\text{exc,hh}} \sum_i \exp\left(-\frac{(E - E_{\text{g}} - E_{\text{el},i} - E_{\text{hh},i} + E_{\text{exc,hh}})^2}{2\sigma^2}\right) \times \frac{\mu_{\text{el,lh}} E_{\text{exc,lh}}}{3} \sum_i \exp\left(-\frac{(E - E_{\text{g}} - E_{\text{el},i} - E_{\text{lh},i} + E_{\text{exc,lh}})^2}{2\sigma^2}\right)\right\} \tag{11}$$

$E_{\text{exc,hh}}$ and $E_{\text{exc,lh}}$ are heavy- and light-hole exciton binding energies, respectively. The ratios $BE_{\text{exc,hh}}/R_{\text{exc,hh}}$ and $BE_{\text{exc,lh}}/R_{\text{exc,lh}}$ express the changes of the oscillator strengths of the excitonic transitions with respect to the 2D case. The values of $E_{\text{exc,hh}}$ and $E_{\text{exc,lh}}$ listed in table 1 are chosen according to [18], [19], and [20]. Our choice of B is based on the assumption that the oscillator strengths are the same as in the 2D case. We suppose the phenomenological broadening σ to increase with increasing energy separation between the excitonic line and the FSL gap, E_{g}(FSL): $\sigma = \sigma_0[1 + C(E - E_{\text{g}}(\text{FSL}))]$.

The calculation of the reflectance requires also the knowledge of the real part of the complex dielectric function $\epsilon_1(E)$. This can be obtained by means of Kramers–Kronig transformation:

$$\epsilon_1(E) = 1 + \frac{2}{\pi}\int_0^\infty \frac{G\epsilon_2(G) - E\epsilon_2(E)}{G^2 - E^2}\,\mathrm{d}G. \tag{12}$$

Formulas (9) and (11) are suitable only for energies close to the FSL gap. $\epsilon_2(E)$ in the more distant region containing the E_1 and E_2 interband transitions is not known. We approximate it in that region by a Lorentzian line:

$$\epsilon_{2\text{B}}(E) = \frac{FE\Gamma}{(E_0^2 - E^2)^2 + E^2\Gamma^2}. \tag{13}$$

The values of the parameters F, Γ and E_0 presented in table 1 are chosen so that firstly, the Kramers–Kronig transform of (13) reproduces the experimental [21] values of the real part of the permittivity of an alloy with the same portion of Al as involved in the FSL in the energy region around 1.96 eV, and secondly, the calculated $\epsilon_2(E)$ matches (13) at 1.769 eV. The integration in equation (12) can be carried out numerically and the model reflectance of the FSL grown on a GaAs substrate can be calculated from the optical constants using the formula for the normal-incidence reflectance of a system consisting of a layer on a substrate. Optical constants of GaAs were taken from [14].

The calculated imaginary and real parts of the dielectric function are shown in figure 4. The calculated reflectance is shown in figure 5, together with the experimental result.

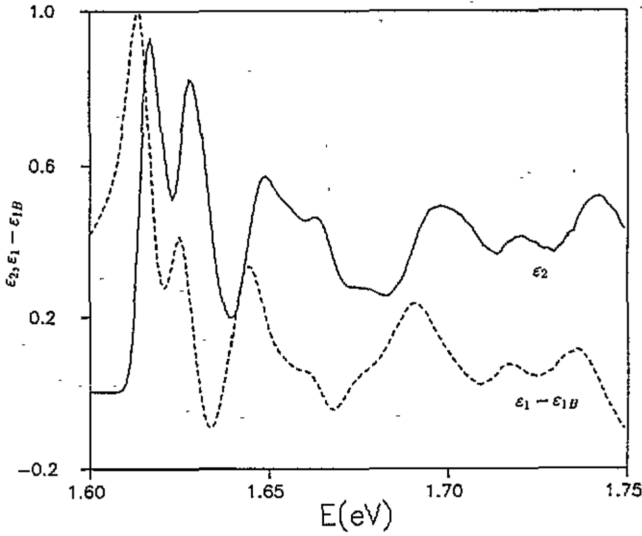

Figure 4. Imaginary part ϵ_2 of the dielectric function (solid line) and the real part ϵ_1 of the dielectric function with the Kramers–Kronig transform ϵ_{1B} of the background Lorentzian subtracted (dashed line) for the FSL S_{12}.

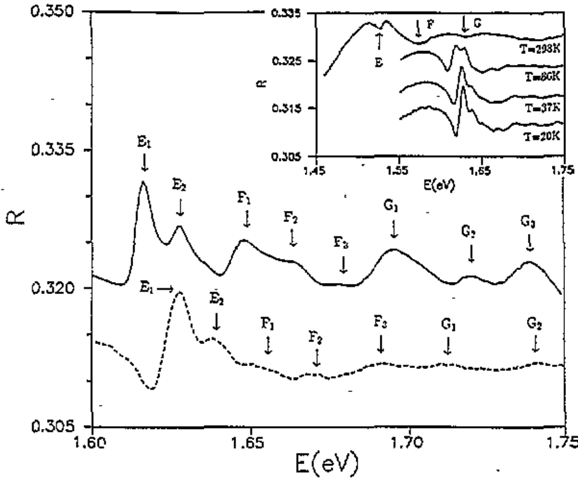

Figure 5. Calculated reflectance spectrum of the FSL S_{12} (solid line) and the measured low-temperature (20 K) reflectance spectrum (dashed line). The structures present in the measured spectrum are labelled in accordance with the labelling of the peaks in the calculated reflectance spectrum: the correspondence is suggested. Inset: temperature evolution of the spectra. The spectra at 37 K, 86 K and 298 K are arbitrarily shifted.

4. Discussion

The shapes of the spectral structures in the reflectance can be understood in the way described in [13]. The change of the reflectance due to a small change of the dielectric function $\Delta\epsilon = \Delta\epsilon_1 + \mathrm{i}\Delta\epsilon_2$ is given by the following formula:

$$\Delta R = \frac{1}{2n}\left(\frac{\mathrm{d}R}{\mathrm{d}k}\Delta\epsilon_2 + \frac{\mathrm{d}R}{\mathrm{d}n}\Delta\epsilon_1\right). \tag{14}$$

Here n and k are refractive and extinction indices of the layer, respectively; $k \ll n$ in the energy interval of interest. The derivatives of R calculated for a model system consisting of a non-absorbing layer with the index of refraction $n(E) = \sqrt{\epsilon_{1\mathrm{B}}(E)}$ on the GaAs substrate are shown in figure 6, where $\epsilon_{1\mathrm{B}}(E)$ is the Kramers–Kronig transform of (13). The arrow labelled by LT shows the low-temperature position of the lowest excitonic transition. Close to the gap the derivative $\mathrm{d}R/\mathrm{d}k$ is small and the reflectance is approximately proportional to $-(\epsilon_1 - \epsilon_{1\mathrm{B}})$ from figure 4. At higher energies the derivative $\mathrm{d}R/\mathrm{d}k$ increases and the first term in equation (14) dominates the reflectance spectrum, which displays the series of peaks in ϵ_2 from figure 4.

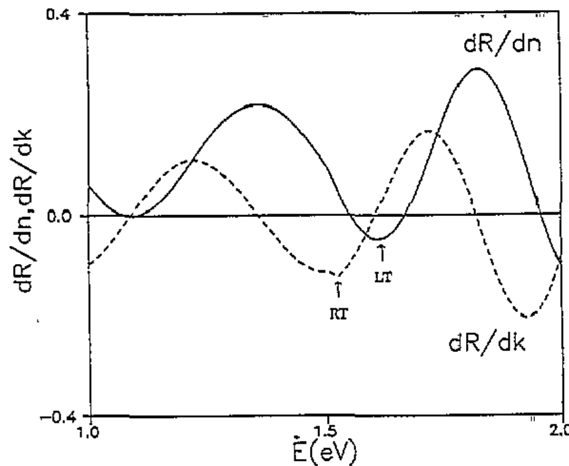

Figure 6. The derivatives of the reflectance R for a model system consisting of a non-absorbing layer of thickness $d = 326$ nm with the index of refraction $n(E) = \sqrt{\epsilon_{1\mathrm{B}}(E)}$ grown on a GaAs substrate with respect to the index of refraction n and the index of extinction k of the layer. $\epsilon_{1\mathrm{B}}(E)$ is the Kramers–Kronig transform of the background Lorentzian. The arrows labelled by LT and RT show the low-temperature and room-temperature positions of the lowest excitonic transition, respectively.

The reflectance spectrum consists of three groups of peaks: E (E_1, E_2), F (F_1, F_2, F_3), and G (G_1, G_2, G_3). This is connected with the multifractal electron energy spectrum (cf. the energy bands of $(S_7)_\infty$ in figure 2). The FSL contains single wells BAB and double wells BAAB. The groups E and G correspond to bonding and antibonding combinations of states located in neighbouring double wells, respectively. The group F corresponds to states located mainly in isolated double wells. These are separated from the other double wells by single wells. The peaks are predominantly due to heavy-hole excitons with the exception

Table 2. Energies in meV corresponding to the arrows in figure 5 relative to the experimental position of E_1 = 1627 meV.

	E_1	E_2	F_1	F_2	F_3	G_1	G_2	G_3
Theory	−11	0	21	36	51	68	93	112
Theory + 11 meV	0	11	32	47	62	79	104	123
Experiment	0	11	27	42	63	85	113	—

of F_3 which is of light-hole origin. The energy positions of the arrows in figure 5 are given in table 2.

The calculated reflectance is about 1% higher than the measured one. This could be due to the experimental inaccuracy and/or to the approximations of the background dielectric function.

Nearly all the features seen in the measured spectrum can be assigned to the computed structures. The onset of the superlattice absorption (the peak denoted by E_1 and the preceding dip) is shifted by about 11 meV towards lower energies in the calculated spectrum. This shift might have the following explanation. The EFA is based on the assumption that the envelope functions vary slowly at the scale of the lattice parameter. This is not justified in our case: the envelope functions do vary dramatically inside each barrier and the barrier thickness is only 3 mL. The interwell coupling may thus be overestimated in the EFA and the ground-state energy underestimated. The calculated distances between the spectral structures are in very good agreement with the experiment as seen from table 2.

The calculation underestimates the oscillator strengths connected with the transitions resulting in the structures denoted by E_1 and E_2. This may be partially due to the enhancement of the exciton reduced mass suggested by Masumoto *et al* [23] for the absorption spectra of narrow quantum wells.

The strengths connected with the transitions resulting in the structures denoted by F_1, F_2, G_1 and G_2 are overestimated in the calculated reflectance. There are considerable differences between the electron and hole localizations as confirmed by the calculation of some of the overlap integrals (8). For example, the squared overlap between the wave functions of electrons and heavy holes corresponding to the centre of the spectrum is only 0.74 instead of unity. We suggest that the approximation (8) neglecting the transitions between electron and hole states with different indices is one of the reasons for the overestimation quoted above. The other reason may be that the corresponding exciton states are less localized and consequently the oscillator strengths are smaller [23].

The temperature evolution of the spectra is shown in the inset of figure 5. Note that all the structures labelled in the low-temperature spectra can be identified also at 37 K. With increasing temperature the spectral structures shift towards lower energies and their broadening increases. The three branches E, F and G are present up to room temperature but their fine structure vanishes at about 100 K. The room-temperature lineshapes can be understood with the help of figure 6 since the temperature shift of the interference background is distinctly lower than the shift of the absorption structure. At room temperature the absorption edge is located at about 1520 meV (the point labelled by RT in figure 6). In that region the derivative $\mathrm{d}R/\mathrm{d}k$ is negative and, according to equation (14), a minimum appears in the reflectance spectrum close to the absorption edge.

5. Conclusion

The electronic structure of FSLs was studied theoretically and by means of reflectance

spectroscopy.

The calculations reveal the multifractal properties of the electron energy spectrum and the self-similarity of the wave function of the ground state.

Our measured reflectance spectrum exhibits the hierarchical structure resulting from the branching of the energy spectrum. Three branches can be identified and each of them has an inner structure.

The calculated reflectance spectrum is shifted slightly towards lower energies. The distances between the spectral structures are in very good agreement with the experiment. It is interesting that the EFA yields results in quantitative agreement with the experiment although the barrier thickness is only 3 mL. The theory underestimates the oscillator strengths of the lowest excitonic transitions but those corresponding to the higher ones are overestimated.

Acknowledgment

This work has been financially supported by GA CR (grant No 202/93/2119).

References

[1] Steinhardt P J and Levine D (ed) 1987 *The Physics of Quasicrystals* (Singapore: World Scientific)
[2] Kohmoto M, Sutherland B and Tang C 1987 *Phys. Rev.* B **35** 1020
[3] Merlin R, Bajema K, Clarke R, Juang F Y and Bhattacharya B K 1985 *Phys. Rev. Lett.* **55** 1768
[4] Merlin R 1988 *IEEE J. Quantum Electron.* **QE-24** 1791
[5] Garriga M 1990 *PhD Thesis* Max-Planck-Institut für Festkörperforschung, Stuttgart
[6] Garriga M, Brey L, Nagle J and Ploog K 1988 *19th Int. Conf. on Physics of Semiconductors (Warsaw, 1988)* ed W Zawadzki (Warsaw: Institute of Physics, Polish Academy of Sciences) p 263
[7] Laruelle F and Etienne B 1988 *Phys. Rev.* B **37** 4816
[8] Yamaguchi A A, Saiki T, Tada T, Ninomiya T, Misawa K, Kobayashi T, Kuwata-Gonokami M and Yao T 1990 *Solid State Commun.* **75** 955
[9] Bastard G 1988 *Wave Mechanics Applied to Semiconductor Heterostructures* (Les Ulis: Halsted)
[10] Hirose K, Ko D Y K and Kamimura H 1992 *J. Phys.: Condens. Matter* **4** 5847
[11] Vogl P, Hjalmarson H P and Dow J D 1983 *J. Phys. Chem. Solids* **44** 365
[12] Kohmoto M, Kadanoff L and Tang C 1983 *Phys. Rev. Lett.* **50** 1870
[13] Humlíček J, Lukeš F, Navrátil K, Garriga M and Ploog K 1989 *Appl. Phys.* A **49** 407
[14] Palik E D (ed) 1985 *Handbook of Optical Constants of Solids* (New York: Academic) p 547 (Si), p 429 (GaAs)
[15] Halsey T C, Jensen M H, Kadanoff L P, Procaccia I and Shraiman B I 1986 *Phys. Rev.* A **33** 1141
[16] Munzar D 1993 *Phys. Status Solidi* b **175** 395
[17] Lederman F L and Dow J D 1976 *Phys. Rev.* B **13** 1633
[18] Grundmann M and Bimberg D 1988 *Phys. Rev.* B **38** 13486
[19] Campi D and Villavecchia C 1992 *IEEE J. Quantum Electron.* **28** 1765
[20] Mathieu H, Lefebvre P and Christol P 1992 *Phys. Rev.* B **46** 4092
[21] Palik E D (ed) 1991 *Handbook of Optical Constants of Solids II* (New York: Academic) p 513 (GaAlAs)
[22] Humlíček J, Lukeš F and Ploog K 1991 *Superlatt. Microstruct.* **9** 133
[23] Masumoto Y, Matsuura M, Tarucha S and Okamoto H 1985 *Phys. Rev.* B **32** 4275
[24] *Landolt–Börnstein New Series* 1987 Group III, vol 22a, ed O Madelung and M Shultz (Berlin: Springer) p 82 (GaAs), p 63 (AlAs)